Forced amyloidogenic cooperativity of structurally incompatible peptide segments: Fibrillization behavior of highly aggregation-prone A-chain fragment of insulin coupled to all-L, and alternating L/D octaglutamates

Robert Dec,[1,2] Róża Okoń,[1] Wojciech Puławski,[3] Matylda Wacławska,[1] and Wojciech Dzwolak[1*,4]

[1]Faculty of Chemistry, Biological and Chemical Research Centre, University of Warsaw, Pasteur Street 1, 02-093 Warsaw, Poland.

[2]Physical Chemistry I - Biophysical Chemistry, Department of Chemistry and Chemical Biology, TU Dortmund University, Otto-Hahn Street 4a, 44227 Dortmund, Germany (Present address)

[3]Bioinformatics Laboratory, Mossakowski Medical Research Institute, Polish Academy of Sciences, Pawinskiego Street 5, 02-106 Warsaw, Poland

[4]Institute of High Pressure Physics, Polish Academy of Sciences, Sokołowska Street 29/37, 01-142 Warsaw, Poland

* Corresponding author:

Phone: +48 22 552 6567;

Fax: +48 22 552 4029 ;

E-mail: wdzwolak@chem.uw.edu.pl

Abstract

Self-aggregation of individual polypeptide chains into amyloid fibrils is driven by interactions between amyloidogenic segments of whole proteins. The interplay between aggregation-prone and aggregation-resistant fragments within a single polypeptide chain is not well understood. Here, we examine fibrillization behavior of two designed chimeric peptides, $ACC_{1-13}E_8$ and $ACC_{1-13}E_{8(L/D)}$, in which the highly amyloidogenic fragment of insulin's A-chain (ACC_{1-13}) is extended by an octaglutamate segment composed of *all*-L (E_8), or alternating L/D residues ($E_{8(L/D)}$). As separate entities, ACC_{1-13} readily forms fibrils with the infrared features of parallel β-sheet structure while acidified E_8 forms so-called β_2-aggregates consisting of antiparallel β-sheets and manifesting distinctly in the amide I band infrared region. This contrasts with profoundly aggregation-resistant behavior of $E_{8(L/D)}$ peptide although the alternating L/D motif has been hypothesized as compatible with aggregated α-sheets. $ACC_{1-13}E_8$ and $ACC_{1-13}E_{8(L/D)}$ peptides are equally prone to fibrillization when the electrostatic repulsion between dissolved monomers is prevented either by lowering pH, or in the presence of Ca^{2+} ions. In the aggregated states, both $ACC_{1-13}E_8$ and $ACC_{1-13}E_{8(L/D)}$ reveal the infrared characteristics of ordered parallel β-sheet structure with no spectral features attributable to β_2-aggregates ($ACC_{1-13}E_8$) or α-sheets ($ACC_{1-13}E_{8(L/D)}$). Hence, the preferred structural pattern of ACC_{1-13} segment not only overrides the tendency of E_8 to form the antiparallel β_2-structure but also enforces formation of β-sheet structure within the $E_{8(L/D)}$ segment which on its own is entirely refractory to aggregation. We demonstrate how an alternating L/D sequence can be effectively forced to become a part of highly ordered amyloid structure scaffolded by an *all*-L amyloidogenic segment. Our study shows how the overall amyloidogenic characteristics of a larger hybrid sequence may be impacted and controlled by the properties of its most aggregation-prone part.

Keywords:

Amyloid stretch; Chimeric peptide; Hydrogen bond with bifurcated acceptor; β-strand direction; Homopolypeptide; α-sheet

1. Introduction

The self-assembly of polypeptide chains into highly ordered amyloid fibrils, whose main structural motif is based on an intermolecular β-sheet structure assembled along the fibril axis, is a generic transition accessible to structurally and genetically unrelated proteins, as well as synthetic peptides and homopolypeptides [1-3]. The main rationale for undertaking studies on amyloidogenesis arises from the fact that abnormal amyloid deposits are associated with various degenerative maladies including Alzheimer's disease, Parkinson's disease and diabetes mellitus type II [3-5]. Whether mature amyloid fibrils are the most detrimental protein species may depend on the exact type of disease and is often debated. Nevertheless, gaining insights into the intricate nature of the phenomenon of amyloidogenesis and the spatial structures of amyloid fibrils could translate into development of new therapeutic strategies [6-7]. Depending on the type of parent protein (or peptide) and conditions of aggregation, the fibrils may be non-toxic while featuring unique levels of thermodynamic and environmental stability often coupled to desirable mechanical properties [8-9]. These properties have been harvested by living organisms, as reported in many studies on biologically functional amyloid fibrils [10-12].

Amyloidogenesis is often driven by a relatively short segment of protein's amino acid sequence with a particular propensity to form fibrils (sometimes termed *amyloid stretch* [13]). There are certain intuitive traits of these fragments such as propensity of the individual residues to form β-sheet, hydrophobicity, lack of proline residues, etc. Mapping such fragments within larger portions of primary structure allows one to predict with some success the overall amyloidogenicity of the parent protein [14-16]. However, the interplay of amyloidogenic segments with other parts of the protein which are less prone to aggregation is very complex, far from being understood and its outcome is often difficult to predict. Recently, we have shown that the N-terminal segment of

bovine insulin's A-chain (Fig. 1) encompassing the intrachain Cys6-Cys11 disulfide bond, ACC_{1-13}, is a very powerful amyloid stretch enforcing an in-register parallel β-sheet structure upon fibrillization [17-19].

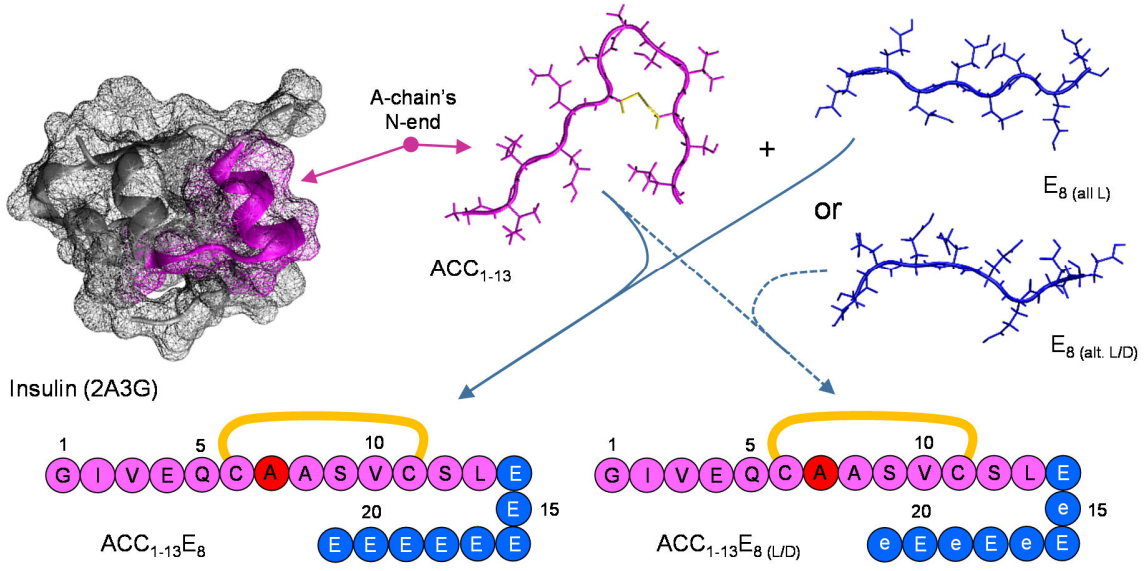

Figure 1. Design of $ACC_{1-13}E_8$ and $ACC_{1-13}E_{8(L/D)}$ peptides. The amino acid sequence of the N-terminal segment of bovine insulin's A-chain (the first 13 residues) was extended at the C-end by additional 8 glutamate residues either *all*-L ($ACC_{1-13}E_8$) or alternating L/D ($ACC_{1-13}E_{8(L/D)}$) enantiomers. D-type residues are marked in small letters while L-type are in capital letters.

Hypothetically, this same fragment contributes significantly to the known aggregation propensity of insulin [20]. When engineered into primary structures of synthetic peptides ACC_{1-13} confers them with very strong propensity to form amyloid fibrils under permissive conditions [18, 21]. The remarkable structural adaptability of ACC_{1-13} has been demonstrated for a pair of linear chimeric peptides whose sequences correspond to ACC_{1-13} attached to N-, or C-ends of the marginally

amyloidogenic N-terminal fragment of insulin's B-chain [18]. The merged segments of N-terminal regions of insulin's A- and B-chains proved highly amyloidogenic. The infrared features of the resulting fibrils indicate a parallel arrangement of individual β-strands. Since the B-chain-derived peptides also form fibrils with the parallel β-sheet infrared characteristics there was no obvious structural incompatibility of both segments as far as fibrillization of these peptides is concerned. Hence, it became of interest to us to design an analogous chimeric system in which ACC_{1-13} is coupled to an amyloidogenic segment which on its own would form antiparallel β-sheet with distinct infrared features. Various homopolypeptides are known to form amyloid-like fibrils with infrared features indicative of antiparallel β-sheet [22-23]. The case of poly-L-glutamic acid (poly-E) is particularly interesting. In an appropriately acidified environment, poly-E chains self-assemble into so-called β_2-fibrils exhibiting very unique infrared features [24-25]. Namely, the amide I vibrational band is dramatically shifted to approximately 1600 cm^{-1} which has been explained by the presence of three-centered hydrogen bonds coupling side chain's carboxyl and main chain –NH groups as hydrogen donors to main chain >C=O groups as bifurcating acceptors [26-27]. This unusual hydrogen bonding pattern is compatible with an antiparallel arrangement of individual strands, but it also entails an unusual compression of the aggregate in the direction orthogonal to the β-sheet's plane. It has been also demonstrated that *all*-L oligoglutamates of various lengths (even as short as E_4 [28-29]) would readily form β_2-fibrils upon lowering the pH. In this study, we selected octaglutamate as a seemingly incompatible amyloidogenic segment to be merged with the insulin's ACC_{1-13} fragment in order to study interplay of these two fragments in the amyloidogenic context. We have investigated chimeric peptides in which E_8 were composed of *all*-L (compatible with the β_2-aggregates) and alternating L/D residues. The latter pattern is potentially compatible with the α-sheet structure [30-33], a rather exotic secondary structure hypothesized to be involved in formation of certain amyloid-like fibrils [34-35]. Using infrared

absorption spectroscopy, atomic force microscopy (AFM) and kinetic assays based on Thioflavin T (ThT) fluorescence we demonstrate that in either case, the insulin fragment exerts strict control over the conformational transition within the oligoglutamate segment. The results highlight a novel approach to the problem of thermodynamic frustration within amyloid fibrils.

2. Results and Discussion

As an integral part of the folded insulin monomer, ACC_{1-13}, the disulfide-constrained N-terminal fragment of insulin's A-chain, remains in the α-helical conformation (Fig. 1). However, as a separate entity in aqueous solution, ACC_{1-13} is disordered, yet with a very pronounced tendency to self-aggregate into amyloid fibrils with the infrared features of a predominantly parallel β-sheet structure ([17-20]). As our previous study has shown, ACC_{1-13} reveals a remarkable capacity to *activate* amyloidogenicity in marginally aggregation-prone peptide segments. In this respect, ACC_{1-13} is very versatile: the amyloidogenic transfer takes place regardless of whether the non-amyloidogenic segment is linked to ACC_{1-13} at the N- or C-termini, or laterally via a disulfide bridge [18]. Following the recent work on the ACC_{1-13}–oligolysine chimer [21], we have chosen to attach oligoglutamate E_8 / $E_{8(L/D)}$ segments at ACC_{1-13} C-end.

Coulombic repulsion is expected to prevent self-aggregation of ACC_{1-13} – oligoglutamate chimers at sufficiently high pH. In a preliminary experiment, the fibrillization tendency of $ACC_{1-13}E_8$ as a function of pH was examined using the ThT-fluorescence assay. The kinetic trajectories depicting the progress of the fibrillization shown in Fig. 2A indicate that there is no detectable aggregation of $ACC_{1-13}E_8$ at the neutral pH, however the process is already detectable at pH 5.2 even though it occurs after a significant lag-time of 5 hours. Further acidification of the peptide solution triggers explosive fibrillization manifesting in very short (and therefore difficult to quantify) lag-times. The appearances of the initial sections of the kinetic trajectories collected at pH 4.1, 3.2, and 2.1 are very similar suggesting that once most of glutamate side chains become protonated, further acidification of the environment has little impact on the course of aggregation. We note that the final plateau of ThT signal detected after 24 hours in the three most acidified samples is roughly 3-4 times higher than in the case of aggregation induced at pH 5.2.

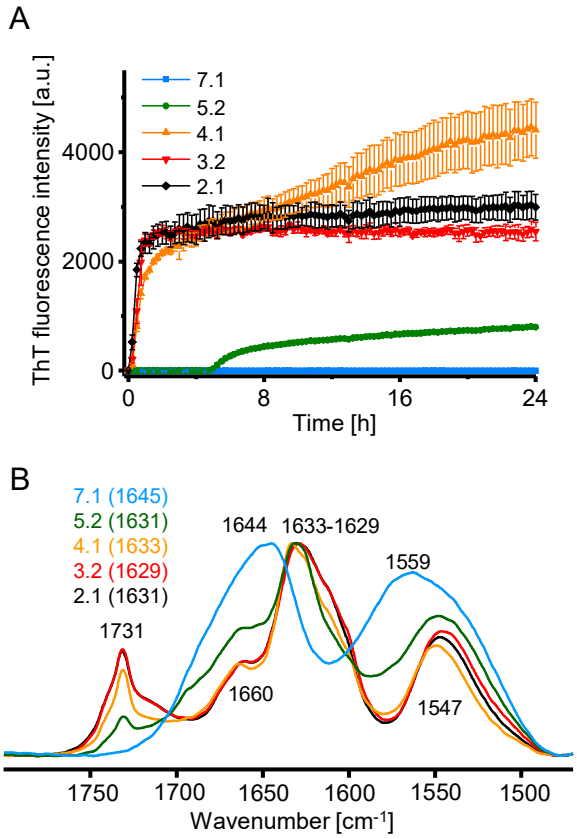

Figure 2. (A) *De novo* fibrillization kinetics of $ACC_{1\text{-}13}E_8$ (0.216 mM, 37 ºC, 300 rpm) probed by ThT fluorescence assay at various pH values as indicated. (B) Infrared spectra of the aggregates collected at the end of the kinetic experiment, spectral positions of the amide I band maxima are indicated in parenthesis.

The FT-IR spectra of peptide samples collected at the end of the kinetic experiment and shown in Fig. 2B confirm that the aggregation and precipitation of $ACC_{1\text{-}13}E_8$ is accompanied by the conformational transition to β-sheet structure. The broad amide I band at 1644 cm^{-1} indicative of structural disorder is observed only for the non-aggregated peptide at pH 7.1 The band is flanked by another one at 1559 cm^{-1} which arises from the overlapping amide II band and antisymmetric stretches of ionized carboxyl groups in glutamate side chains ([36]). In the case of low-pH-induced aggregates of $ACC_{1\text{-}13}E_8$, the amide I band frequency is shifted to 1629-1633 cm^{-1} range diagnostic

of parallel β-sheet. This spectral change occurs *in phase* with the emergence of sharp peak at 1731 cm^{-1} assigned to protonated carboxyl groups and the simultaneous decrease of the signal arising from ionized carboxyl groups with the remaining amide II band at 1547 cm^{-1}. Interestingly, in the case of aggregate formed at pH 5.2, the main β-sheet-assigned spectral component of the amide I band is flanked at the high frequency side by an enlarged signal at 1660 cm^{-1} implying a higher proportion of turns relative to β-sheets as compared to the aggregates formed at lower pH values. This is accompanied by the visibly reduced absorption intensity at 1731 cm^{-1} while some residual absorption by ionized carboxyl groups is observed below 1600 cm^{-1}. All these traits suggest that at the borderline permissive pH, $ACC_{1\text{-}13}E_8$ may form aggregates less ordered on the level of secondary structure which are capable of accommodating partly charged glutamate side chains.

Subsequently, we examined fibrillization properties of both $ACC_{1\text{-}13}E_8$ and $ACC_{1\text{-}13}E_{8(L/D)}$ at two selected pH values: aggregation-inducing (pH 4), and aggregation-preventing pH (6.1). At pH 6.1 it was also possible to introduce Ca^{2+} ions in the ten-fold molar excess as a potential alternative-to-low-pH trigger of aggregation. The idea that multivalent metal cations could trigger fibrillization of $ACC_{1\text{-}13}E_8$ / $ACC_{1\text{-}13}E_{8(L/D)}$ is conceptually similar to that explored in our recent work on an analogous $ACC_{1\text{-}13}K_8$ peptide whose fibrillization is triggered by oligoanions such as ATP [21]. While the presence of ions can affect amyloidogenesis in various and nuanced ways including the Hofmeister-series-related effects (e.g. [37]) here a more straightforward scenario is verified in which capture of Ca^{2+} by ionized carboxyl groups allows for a charge-compensation and a cooperative self-assembly of fibrils trapping the metal ions. Fibrillization of both chimeric peptides at pH 4, and at pH 6.1 in the presence of dissolved $CaCl_2$, was compared with the behavior of their building segments ($ACC_{1\text{-}13}$, E_8, $E_{8(L/D)}$). The key kinetic data on aggregation progress in various

peptide systems along with the infrared spectra of the precipitated pellets collected at the end of the kinetic experiments are shown in Fig. 3.

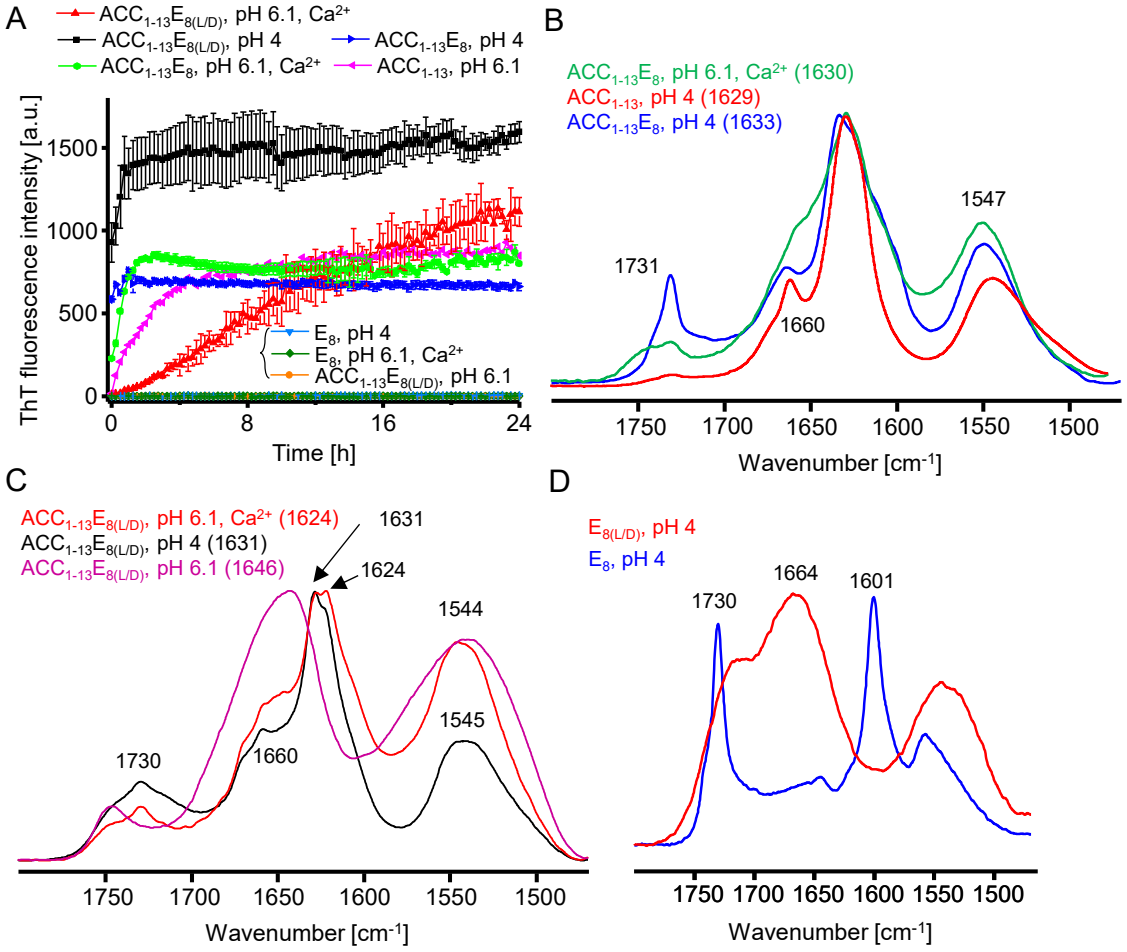

Figure 3. (A) *De novo* fibrillization kinetics of $ACC_{1\text{-}13}E_8$ and $ACC_{1\text{-}13}E_{8(L/D)}$ (0.216 mM, 37 ºC, 300 rpm) and separate segments $ACC_{1\text{-}13}$, E_8 under various pH conditions and in the presence and absence of Ca^{2+} (10-fold molar excess) probed by ThT fluorescence assay. (B-C) Infrared spectra of aggregates collected at the end of the kinetic experiment, positions of the amide I band maxima are indicated in parenthesis. (D) Infrared spectra of E_8 and $E_{8(L/D)}$ peptides (0.3 mg/ml, pH 4) subjected to 48h incubation at 60 ºC.

Clearly, at pH 4 both $ACC_{1-13}E_8$ and $ACC_{1-13}E_{8(L/D)}$ convert into ThT-positive aggregates very rapidly and at very similar timescales. The ThT signal final plateau is approximately twice higher in the case of $ACC_{1-13}E_{8(L/D)}$ which, given the identical concentrations of both peptides and ThT, could imply that either dye-fibril binding affinity is higher or that the local geometries of ThT-binding moieties on $ACC_{1-13}E_{8(L/D)}$ aggregates allow for higher quantum yields [38-39]. Furthermore, at the pH 6.1, at which $ACC_{1-13}E_8$ and $ACC_{1-13}E_{8(L/D)}$ do not aggregate due to the Coulombic repulsion (in contrast to the separate charge-depleted ACC_{1-13} segment) the aggregation of either peptide is apparently triggered by the addition of 10-fold molar excess of Ca^{2+} ions. This result confirms our hypothesis that binding of multivalent cations could constitute an alternative to glutamate-protonation pathway to compensate charge and allow $ACC_{1-13}E_8$ / $ACC_{1-13}E_{8(L/D)}$ to aggregate. We note that, at least under the conditions of this study, aggregation induced by the presence of Ca^{2+} ions is slower than that induced by low pH. There could be many factors responsible for this effect – from the slower diffusion of Ca^{2+} versus H_3O^+ to a local deceleration of the conformational transition involving packing of multiple cations. The fact that the relative retardation of Ca^{2+}-induced aggregation is more pronounced for $ACC_{1-13}E_{8(L/D)}$ than $ACC_{1-13}E_8$ suggests that the diffusion factor is not the rate determining step of the overall transition. Importantly, when separated from the ACC_{1-13} stretch neither E_8 nor $E_{8(L/D)}$ form aggregates under these conditions of concentration and temperature regardless of whether low pH, or Ca^{2+} are used as the triggers. However, only when the acidified E_8 sample is incubated at 60 ^oC for a prolonged period of time the aggregation does occur (as opposed to the $E_{8(L/D)}$ case).

The infrared spectra of various peptides collected at the end of the kinetic experiment are shown in panels B and C of Fig. 3. The wavenumbers corresponding to the main component of the amide I bands of aggregated $ACC_{1-13}E_8$ and $ACC_{1-13}E_{8(L/D)}$ are within the range indicative of parallel β-

sheet. We notice, however, that the corresponding spectral contours are broadened, as compared to the $ACC_{1\text{-}13}$ aggregate (Fig. 3B). The broadening is more evident in the Ca^{2+}-induced than in the low-pH-induced aggregates. This observation may be cautiously interpreted as a lower degree of conformational homogeneity in the aggregated peptides encompassing the oligoglutamate segments. The 1731 cm^{-1} peak which is very sharp in the spectrum of $ACC_{1\text{-}13}E_8$ precipitated at pH 4 is still visible in the Ca^{2+}-induced aggregate although significantly broadened and shifted to higher frequencies. This implies a higher degree of local order around Glu side chains in the former case, and that even at the close-to-neutral pH some of the glutamate side chains within the Ca^{2+}-stabilized aggregate become protonated allowing thereby to reduce the local electrostatic frustration caused by the dense spatial packing. In the spectra of $ACC_{1\text{-}13}E_{8(L/D)}$ aggregates shown in Fig. 3C, there is no indication that low pH induces a similar degree of structural order involving the –COOH groups. Hence, the alternating L/D pattern may be less permissive to effective dumping of structural fluctuations of these side-chains. More importantly, in the case of $ACC_{1\text{-}13}E_{8(L/D)}$, there is no evidence of resolved bands at, and above 1670 cm^{-1} which, according to earlier computational ([40]) and experimental ([32, 41]) works, would be indicative of the α-sheet structure. Instead, the slightly split amide I band's component (1624/1631 cm^{-1}) suggests distinct patterns of transition dipole couplings / hydrogen bonds from those present in the β-sheets assembled from $ACC_{1\text{-}13}E_8$ strands. As aforementioned, a prolonged incubation at 60 ^oC of acidified E_8 solution was necessary to trigger a conformational transition which led, predictably, to aggregates revealing the very characteristic spectral features of β_2-fibrils. The densely packed antiparallel β-sheets with the unusual hydrogen bonds involving bifurcating carbonyl acceptors give rise to the very narrow and dramatically red-shifted (~ 1600 cm^{-1}) amide I band flanked by a strong and sharp –COOH peak at 1730 cm^{-1} (Fig. 3D). On the other hand, $E_{8(L/D)}$ peptide does not undergo any detectable conformational transition. It appears that, in this case, the β_2-structure may be inaccessible due to

steric conflicts while the hypothetically feasible for an L/D chiral pattern ([32]) α-sheet conformation is not formed due to the innate thermodynamic instability (arising from the significant electric dipole moment of a multi-strand α-sheet [42]).

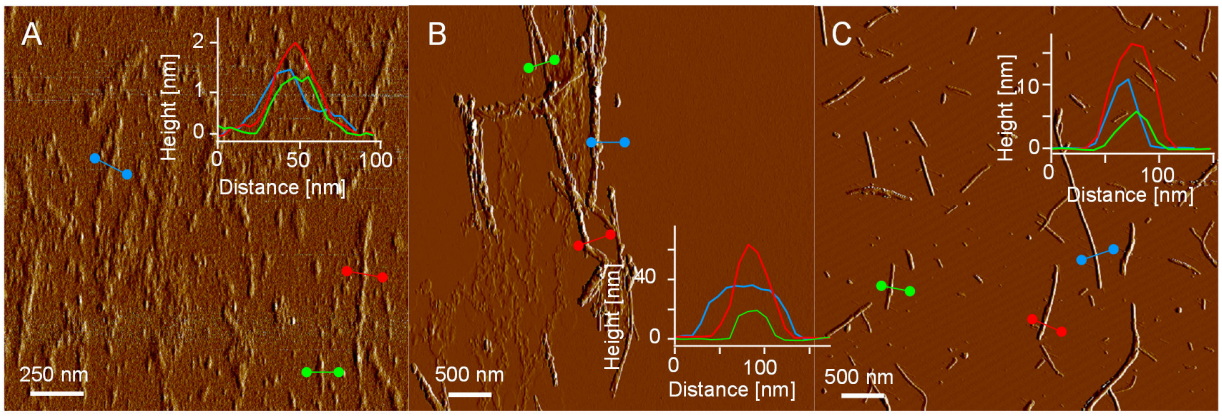

Figure 4. AFM amplitude images of aggregates of $ACC_{1\text{-}13}E_8$ (A) and $ACC_{1\text{-}13}E_{8(L/D)}$ (B) formed at pH 4 and in the absence of Ca^{2+}, and of $ACC_{1\text{-}13}E_{8(L/D)}$ at pH 6.1 and in the presence of 10-fold molar excess of Ca^{2+} (C). Superimposed are cross-sections of selected specimen.

AFM amplitude images of selected fibrillar specimen of $ACC_{1\text{-}13}E_8$ and $ACC_{1\text{-}13}E_{8(L/D)}$ formed under various conditions are shown in Fig. 4. Fibrils of $ACC_{1\text{-}13}E_8$ induced at the low pH are rather thin (~ 2 nm in diameter according to the corresponding height image) and brittle whereas fibrils grown in the presence of Ca^{2+} are significantly thicker (~10-40 nm for $ACC_{1\text{-}13}E_8$, ~10 nm for $ACC_{1\text{-}13}E_{8(L/D)}$) suggesting that each specimen is likely to consist of several laterally aligned individual protofilaments. Perhaps such a superstructural organization may be rationalized by the fact that a bivalent Ca^{2+} ion could be simultaneously coordinated by glutamate carboxyl groups from different protofilaments. The image in Fig 4C along with the infrared data shown in Fig. 3C provide convincing evidence that the $E_{8(L/D)}$ segment, despite its non-amyloidogenic character, may

be forced to become a part of a highly ordered fibrillar structure when coupled to a strong amyloid stretch. The self-assembly of $ACC_{1\text{-}13}E_8$ / $ACC_{1\text{-}13}E_{8(L/D)}$ is conditioned upon mitigation of the Coulombic repulsion between peptide monomers which is achieved either by protonation of glutamate side chains or incorporation of charge-compensating Ca^{2+} ions. The conformational disorder→β-sheet transition occurs *in phase* with the fibrillization, as may be inferred from the far-UV CD spectra of diluted peptide samples collected before and immediately after acidification (or titration with $CaCl_2$) presented in Fig. 5.

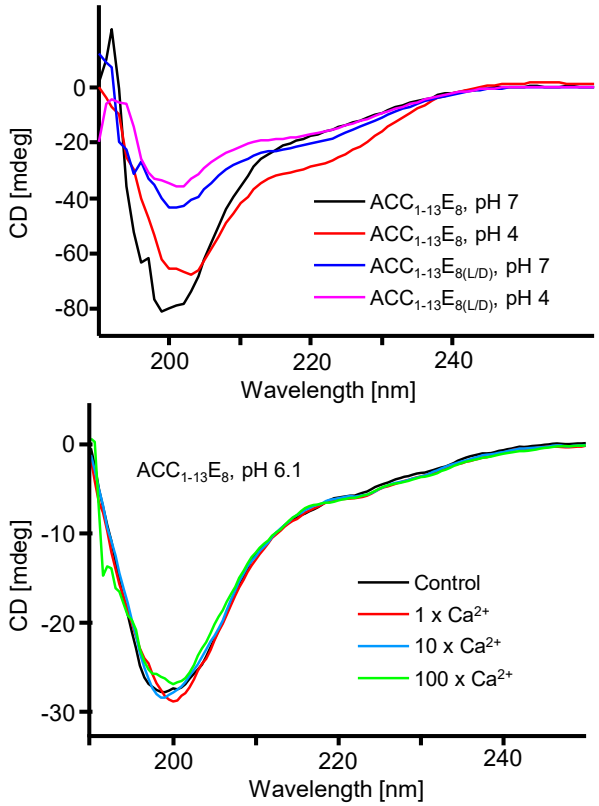

Figure 5. Far-UV CD spectra of (top panel) dissolved $ACC_{1\text{-}13}E_8$ and $ACC_{1\text{-}13}E_{8(L/D)}$ peptides prior to aggregation and before and after acidification, (bottom) $ACC_{1\text{-}13}E_8$ dissolved at pH 6.1 in the presence of increasing molar excess of Ca^{2+} (peptide concentration 0.21 mg/ml, 1 mm quartz cuvette).

Under these conditions the conformational state of monomers prior to aggregation is reported. It is clear that both peptides remain in the disordered state, i.e. the transition to β-sheet structure occurs at longer time-scales necessary for the diffusion of monomers and subsequent fibrillization.

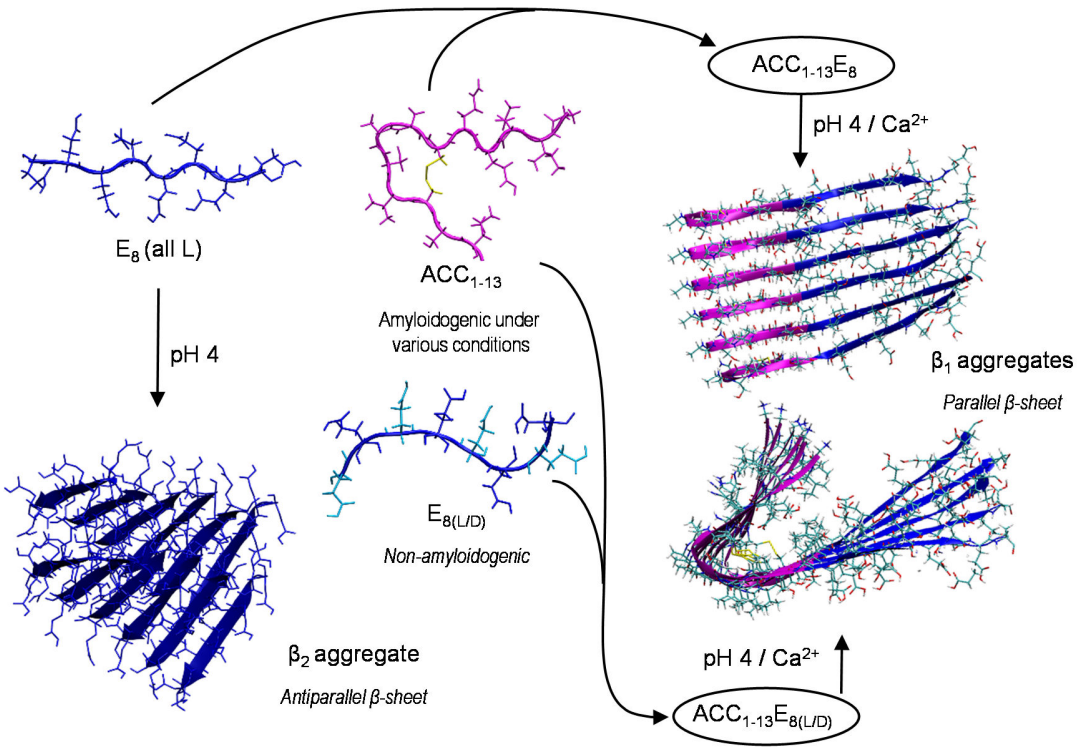

Figure 6. Scheme of the aggregation pathways of the peptides investigated in this study. According to the IR data fibrils of $ACC_{1-13}E_{8(L/D)}$, $ACC_{1-13}E_8$, and ACC_{1-13} consist of parallel β-sheet structure. As a separate entity, E_8 peptide forms antiparallel β-sheets with the untypical hydrogen bonds involving bifurcating carbonyl acceptors whereas $E_{8(L/D)}$ is not amyloidogenic at all.

3. Conclusions

In this study, we have investigated amyloidogenic properties of two chimeric peptides $ACC_{1-13}E_8$ and $ACC_{1-13}E_{8(L/D)}$ engineered by merging the amino acid sequence of the insulin-derived powerful

and versatile amyloid stretch, ACC_{1-13}, with two homooligopeptides: E_8 and $E_{8(L/D)}$. Of these two, E_8 is moderately amyloidogenic at low pH but with the propensity to form antiparallel β_2-type of aggregate which is structurally incompatible with ACC_{1-13} fibrils. On the other hand, $E_{8(L/D)}$ is not amyloidogenic at all although its alternating L/D chiral pattern could be, in principle, permissive to the α-sheet conformation, the exotic secondary fold hypothesized to be involved in formation of some amyloid structures. Our results summarized in Fig. 6 provide strong evidence of the transfer of amyloidogenicity from ACC_{1-13} to the oligo-glutamate segments. The E_8 / $E_{8(L/D)}$ fragments are forced to participate in the fibrillar structure formed by the chimeric peptides. The innate preference of E_8 for β_2-aggregates is overridden by ACC_{1-13} tendency to form regular parallel β-sheet structure. While a multi-strand α-sheet conformation is expected to be thermodynamically less stable than the β-sheet structure, hypothetically – it could have been stabilized in $E_{8(L/D)}$ segments upon merger with ACC_{1-13}. However, the infrared features of $ACC_{1-13}E_{8(L/D)}$ suggest that a highly ordered β-sheet conformation involving both these segments is formed, instead. Our work provides a very clear example of an interplay between more and less amyloidogenic segments within a larger polypeptide fragment. It also shows how interactions between multivalent metal cations (long suspected of playing a role in pathogenic protein aggregation *in vivo* [43-44]) and peptides become fortified when the peptides become amyloidogenic and fibrillization is conditioned upon incorporations of these cations. We believe that further studies on analogous to $ACC_{1-13}E_8$ chimeric peptides could provide crucial insights into how local charge compensation through the binding of multivalent ions could affect the fibrillization properties of strongly charged, yet aggregation-prone proteins. Shedding light on these processes will deepen our understanding of the *in vivo* formation of biologically and clinically important amyloid deposits and is expected to facilitate development of new therapeutic strategies in amyloid-related diseases.

4. Materials and Methods

4.1. Peptides

Peptides $ACC_{1\text{-}13}E_8$ (GIVEQCAASVCSLEEEEEEEE) and $ACC_{1\text{-}13}E_{8(L/D)}$ (GIVEQCAASVCSLeEeEeEeE, D-amino acids are shown in lowercase letters) were designed by extending the first 13 N-terminal residues of bovine insulin's A-chain at the C-end by additional segments of 8 glutamate residues. In the case of $ACC_{1\text{-}13}E_8$, all glutamate residues are L-type, while in $ACC_{1\text{-}13}E_{8(L/D)}$, Glu residues at positions 14, 16, 18, and 20 are D-type. In both peptides, insulin's original intrachain Cys6-Cys11 disulfide bond is retained while the Cys7 residue is substituted with Ala (in insulin monomer, Cys7 is involved in an interchain Cys7A-Cys7B disulfide bond). $ACC_{1\text{-}13}E_8$, $ACC_{1\text{-}13}E_{8(L/D)}$, $ACC_{1\text{-}13}$, as well as E_8 (*all*-L) and $E_{8(L/D)}$ (eEeEeEeE) peptides, all without N- or C-terminal modifications, were custom-synthesized by Pepscan (Lelystad, The Netherlands) typically at high purity exceeding 95 % and were delivered by the manufacturer as trifluoroacetic acid (TFA) salts. All other non-peptidic chemicals were from MilliporeSigma (Sigma-Aldrich).

4.2. Sample preparation

Due to the high glutamate content freeze-dried TFA salts (as provided by the manufacturer) of the key peptides used in this study dissolve slowly but completely in slightly alkalized (~ pH 9) water. In this way, stock aqueous solutions of $ACC_{1\text{-}13}E_8$ and $ACC_{1\text{-}13}E_{8(L/D)}$, typically at the 0.433 mM concentration, were obtained. Samples for kinetic measurements were prepared by addition of proper volumes of stock ThT solution (1 mM), and, if necessary, stock $CaCl_2$ solution (4.33 mM, pH 6, or 7) followed by dilution with water and pH-adjustment to the indicated value. The final concentrations of peptide and ThT were 0.216 mM and 20 μM, respectively. If $CaCl_2$ was added, the molar ratio of Ca^{2+} : peptide was kept at 10 : 1. Once the final pH was set the thus prepared

solutions were immediately transferred to the fluorescence plate reader. When control experiments were conducted on the hydrophobic ACC_{1-13} peptide a more elaborate solubilization protocol consisting in initial dispersion of solid peptide sample in 8M guanidine hydrochloride (GdnHCl) solution, pH 9.0 was used. The protocol was described previously [21]. Aggregation of ACC_{1-13} was induced by rapid dilution of concentrated stock solution in 8 M GdnHCl with an excess of appropriately acidified water. As a result, the aggregation of ACC_{1-13} took place in the presence of residual GdnHCl (at 1.33 M concentration), other parameters corresponding to peptide concentration and pH were the same as for other peptides.

4.3. *Fibrillization kinetics (Thioflavin T fluorescence assay)*

ThT-fluorescence-based measurements ($\lambda_{ex.}$ 440 nm / $\lambda_{em.}$ 485 nm) of peptide fibrillization kinetics were carried out on a CLARIOstar® plate reader from BMG LABTECH (Offenburg, Germany) using 96-well black microplates. Typically, each well was filled with a 150 µL portion of freshly prepared peptide solution containing ThT at the 20 µM concentration. Measurements were carried out at 37 ºC and moderate agitation (300 rpm) for at least 24 hours, as specified. Each kinetic trace was calculated as an average from three independently collected trajectories (error bars correspond to standard deviations). Afterward, aggregate samples were collected from the plate washed with portions of water in order to remove excess of salts. Eluted pellets were subjected to atomic force microscopy (AFM), and FT-IR (Fourier transform infrared) spectroscopic measurements.

4.4. Atomic force microscopy (AFM)

Aggregate suspensions were collected from the plate at the end of the kinetic experiment and washed several times with water. Aqueous suspensions of aggregates were further diluted with

water approximately 5 times. A small droplet (10 µl) of such diluted suspension was swiftly deposited onto freshly cleaved mica and left to dry overnight. AFM tapping-mode measurements were carried out using a Nanoscope III AFM from Veeco Instruments (Plainview, NY, USA) and TAP300-Al sensors (res. frequency 300 kHz) from BudgetSensors (Sofia, Bulgaria).

4.5. Attenuated total reflectance (ATR) FT-IR measurements

Centrifuged samples of aggregates collected from the plate at the end of the kinetic experiment were washed several times with equal portions of water. Suspensions of fibrils were deposited and allowed to dry up on diamond surface of single-reflection diamond ATR accessory of Nicolet iS50 FT-IR spectrometer from Thermo Fisher Scientific (Waltham, MA, USA) equipped with a DTGS detector. Typically, for a single ATR FT-IR spectrum 32 interferograms of 2 cm^{-1} resolution were co-added. Due to ambiguity in determining real values of refractive indexes of amyloid aggregates only uncorrected ATR FT-IR data is shown. Spectral data processing was limited to subtracting water vapor spectrum and adjusting 2 point baseline using GRAMS software (Thermo Fisher Scientific).

4.6. Circular dichroism (CD) measurements

For the CD measurements of fresh peptide solutions (typically at the 0.21 mg/ml concentration) 1 mm quartz cuvettes were used. All CD spectra corrected for the buffer signal were acquired at room temperature by accumulation of 5 independent spectra (at 200 nm/s scanning rate) on a J-815 S spectropolarimeter from Jasco Corp. (Tokyo, Japan).

Acknowledgment

This work was supported by the National Science Centre of Poland, grant no. 2017/25/B/ST5/02599.

Conflict of Interest

The authors declare no conflict of interests.

Author Contributions

Wojciech Dzwolak: conception, design, funding acquisition, analysis of data, writing - original draft, project administration; **Robert Dec:** design, research and data collection, analysis of data; **Róża Okoń**: research and data collection, **Wojciech Puławski**: design, analysis of data; **Matylda Wacławska**: research and data collection, analysis of data.

References

[1] Ke, P. C., Zhou, R., Serpell, L. C., Riek, R., Knowles, T. P., Lashuel, H. A., ... & Mezzenga, R. (2020). Half a century of amyloids: past, present and future. Chemical Society Reviews, 49(15), 5473-5509.

[2] Fändrich, M., Fletcher, M. A., & Dobson, C. M. (2001). Amyloid fibrils from muscle myoglobin. Nature, 410(6825), 165-166.

[3] Chiti, F., & Dobson, C. M. (2017). Protein misfolding, amyloid formation, and human disease: a summary of progress over the last decade. Annual review of biochemistry, 86, 27-68.

[4] Eisenberg, D., & Jucker, M. (2012). The amyloid state of proteins in human diseases. Cell, 148(6), 1188-1203.

[5] Hartl, F. U. (2017). Protein misfolding diseases. Annu. Rev. Biochem, 86(1), 21-26.

[6] Ankarcrona, M., Winblad, B., Monteiro, C., Fearns, C., Powers, E. T., Johansson, J., ... & Kelly, J. W. (2016). Current and future treatment of amyloid diseases. Journal of internal medicine, 280(2), 177-202.

[7] Knowles, T. P., Vendruscolo, M., & Dobson, C. M. (2014). The amyloid state and its association with protein misfolding diseases. Nature reviews Molecular cell biology, 15(6), 384-396.

[8] Volpatti, L. R., & Knowles, T. P. (2014). Polymer physics inspired approaches for the study of the mechanical properties of amyloid fibrils. Journal of Polymer Science Part B: Polymer Physics, 52(4), 281-292.

[9] Knowles, T. P., & Mezzenga, R. (2016). Amyloid fibrils as building blocks for natural and artificial functional materials. Advanced materials, 28(31), 6546-6561.

[10] Fowler, D. M., Koulov, A. V., Balch, W. E., & Kelly, J. W. (2007). Functional amyloid–from bacteria to humans. Trends in biochemical sciences, 32(5), 217-224.

[11] Fowler, D. M., Koulov, A. V., Alory-Jost, C., Marks, M. S., Balch, W. E., & Kelly, J. W. (2006). Functional amyloid formation within mammalian tissue. PLoS biology, 4(1), e6.

[12] Oli, M. W., Otoo, H. N., Crowley, P. J., Heim, K. P., Nascimento, M. M., Ramsook, C. B., ... & Brady, L. J. (2012). Functional amyloid formation by Streptococcus mutans. Microbiology, 158(Pt 12), 2903.

[13] Esteras-Chopo, A., Serrano, L., & de la Paz, M. L. (2005). The amyloid stretch hypothesis: recruiting proteins toward the dark side. Proceedings of the National Academy of Sciences, 102(46), 16672-16677.

[14] Tjernberg, L., Hosia, W., Bark, N., Thyberg, J., & Johansson, J. (2002). Charge attraction and β propensity are necessary for amyloid fibril formation from tetrapeptides. Journal of Biological Chemistry, 277(45), 43243-43246.

[15] Yoon, S., & Welsh, W. J. (2004). Detecting hidden sequence propensity for amyloid fibril formation. Protein Science, 13(8), 2149-2160.

[16] Maurer-Stroh, S., Debulpaep, M., Kuemmerer, N., De La Paz, M. L., Martins, I. C., Reumers, J., ... & Rousseau, F. (2010). Exploring the sequence determinants of amyloid structure using position-specific scoring matrices. Nature methods, 7(3), 237-242.

[17] Dec, R., Koliński, M., & Dzwolak, W. (2019). Beyond amino acid sequence: disulfide bonds and the origins of the extreme amyloidogenic properties of insulin's H-fragment. The FEBS journal, 286(16), 3194-3205.

[18] Dec, R., & Dzwolak, W. (2020). Extremely Amyloidogenic Single-Chain Analogues of Insulin's H-Fragment: Structural Adaptability of an Amyloid Stretch. Langmuir, 36(41), 12150-12159.

[19] Dec, R., & Dzwolak, W. (2021). A tale of two tails: Self-assembling properties of A-and B-chain parts of insulin's highly amyloidogenic H-fragment. International Journal of Biological Macromolecules, 186, 510-518.

[20] Piejko, M., Dec, R., Babenko, V., Hoang, A., Szewczyk, M., Mak, P., & Dzwolak, W. (2015). Highly Amyloidogenic Two-chain Peptide Fragments Are Released upon Partial Digestion of Insulin with Pepsin. Journal of Biological Chemistry, 290(10), 5947-5958.

[21] Dec, R., Puławski, W., & Dzwolak, W. (2021). Selective and stoichiometric incorporation of ATP by self-assembling amyloid fibrils. Journal of Materials Chemistry B, 9(41), 8626-8630.

[22] Fändrich, M., & Dobson, C. M. (2002). The behaviour of polyamino acids reveals an inverse side chain effect in amyloid structure formation. The EMBO journal, 21(21), 5682-5690.

[23] Dzwolak, W., Ravindra, R., Nicolini, C., Jansen, R., & Winter, R. (2004). The diastereomeric assembly of polylysine is the low-volume pathway for preferential formation of β-sheet aggregates. Journal of the American Chemical Society, 126(12), 3762-3768.

[24] Itoh, K., Foxman, B. M., & Fasman, G. D. (1976). The two β forms of poly (L-glutamic acid). Biopolymers: Original Research on Biomolecules, 15(3), 419-455.

[25] Fulara, A., Lakhani, A., Wójcik, S., Nieznanska, H., Keiderling, T. A., & Dzwolak, W. (2011). Spiral superstructures of amyloid-like fibrils of polyglutamic acid: an infrared absorption and vibrational circular dichroism study. The Journal of Physical Chemistry B, 115(37), 11010-11016.

[26] Fulara, A., & Dzwolak, W. (2010). Bifurcated hydrogen bonds stabilize fibrils of poly (L-glutamic) acid. The Journal of Physical Chemistry B, 114(24), 8278-8283.

[27] Chi, H., Welch, W. R., Kubelka, J., & Keiderling, T. A. (2013). Insight into the packing pattern of β2 fibrils: a model study of glutamic acid rich oligomers with 13C isotopic edited vibrational spectroscopy. Biomacromolecules, 14(11), 3880-3891.

[28] Hernik, A., Puławski, W., Fedorczyk, B., Tymecka, D., Misicka, A., Filipek, S., & Dzwolak, W. (2015). Amyloidogenic properties of short α-L-glutamic acid oligomers. Langmuir, 31(38), 10500-10507.

[29] Hernik-Magoń, A., Fedorczyk, B., Dec, R., Puławski, W., Misicka, A., & Dzwolak, W. (2017). Effects of terminal capping on the fibrillation of short (L-Glu) n peptides. Colloids and Surfaces B: Biointerfaces, 159, 861-868.

[30] Di Blasio, B., Saviano, M., Fattorusso, R., Lombardi, A., Pedone, C., Valle, V., & Lorenzi, G. P. (1994). A crystal structure with features of an antiparallel α-pleated sheet. Biopolymers: Original Research on Biomolecules, 34(11), 1463-1468.

[31] Bong, D. T., Clark, T. D., Granja, J. R., & Ghadiri, M. R. (2001). Self-assembling organic nanotubes. Angewandte Chemie International Edition, 40(6), 988-1011.

[32] Kellock, J., Hopping, G., Caughey, B., & Daggett, V. (2016). Peptides composed of alternating L-and D-amino acids inhibit amyloidogenesis in three distinct amyloid systems independent of sequence. Journal of molecular biology, 428(11), 2317-2328.

[33] Meng, F., Lu, T., & Li, F. (2019). Stabilization of Solvent to α-Sheet Structure and Conversion between α-Sheet and β-Sheet in the Fibrillation Process of Amyloid Peptide. The Journal of Physical Chemistry B, 123(45), 9576-9583.

[34] Armen, R. S., Alonso, D. O., & Daggett, V. (2004). Anatomy of an amyloidogenic intermediate: conversion of β-sheet to α-sheet structure in transthyretin at acidic pH. Structure, 12(10), 1847-1863.

[35] Shea, D., Hsu, C. C., Bi, T. M., Paranjapye, N., Childers, M. C., Cochran, J., ... & Daggett, V. (2019). α-Sheet secondary structure in amyloid β-peptide drives aggregation and toxicity in Alzheimer's disease. Proceedings of the National Academy of Sciences, 116(18), 8895-8900.

[36] Barth, A. (2000). The infrared absorption of amino acid side chains. Progress in biophysics and molecular biology, 74(3-5), 141-173.

[37] Chaaban, H., Vallooran, J. J., van de Weert, M., & Foderà, V. (2022). Ion-Mediated Morphological Diversity in Protein Amyloid Systems. The journal of physical chemistry letters, 13(16), 3586-3593.

[38] Sulatskaya, A. I., Maskevich, A. A., Kuznetsova, I. M., Uversky, V. N., & Turoverov, K. K. (2010). Fluorescence quantum yield of thioflavin T in rigid isotropic solution and incorporated into the amyloid fibrils. PloS one, 5(10), e15385.

[39] Amdursky, N., Erez, Y., & Huppert, D. (2012). Molecular rotors: what lies behind the high sensitivity of the thioflavin-T fluorescent marker. Accounts of chemical research, 45(9), 1548-1557.

[40] Torii, H. (2008). Amide I infrared spectral features characteristic of some untypical conformations appearing in the structures suggested for amyloids. The Journal of Physical Chemistry B, 112(29), 8737-8743.

[41] Bi, T. M., & Daggett, V. (2018). Focus: Medical Technology: The Role of α-sheet in Amyloid Oligomer Aggregation and Toxicity. The Yale Journal of Biology and Medicine, 91(3), 247.

[42] Xu, S. (2007). Aggregation drives "misfolding" in protein amyloid fiber formation. Amyloid, 14(2), 119-131.

[43] Uversky, V. N., Li, J., & Fink, A. L. (2001). Metal-triggered structural transformations, aggregation, and fibrillation of human α-synuclein: a possible molecular link between Parkinson′ s disease and heavy metal exposure. Journal of Biological Chemistry, 276(47), 44284-44296.

[44] Faller, P., Hureau, C., & La Penna, G. (2014). Metal ions and intrinsically disordered proteins and peptides: from Cu/Zn amyloid-β to general principles. Accounts of chemical research, 47(8), 2252-2259.

Figure Caption

Figure 1. Design of $ACC_{1\text{-}13}E_8$ and $ACC_{1\text{-}13}E_{8(L/D)}$ peptides. The amino acid sequence of the N-terminal segment of bovine insulin's A-chain (the first 13 residues) was extended at the C-end by additional 8 glutamate residues either *all*-L ($ACC_{1\text{-}13}E_8$) or alternating L/D ($ACC_{1\text{-}13}E_{8(L/D)}$) enantiomers. D-type residues are marked in small letters while L-type are in capital letters.

Figure 2. (A) *De novo* fibrillization kinetics of $ACC_{1\text{-}13}E_8$ (0.216 mM, 37 ºC, 300 rpm) probed by ThT fluorescence assay at various pH values as indicated. (B) Infrared spectra of the aggregates collected at the end of the kinetic experiment, spectral positions of the amide I band maxima are indicated in parenthesis.

Figure 3. (A) *De novo* fibrillization kinetics of $ACC_{1\text{-}13}E_8$ and $ACC_{1\text{-}13}E_{8(L/D)}$ (0.216 mM, 37 ºC, 300 rpm) and separate segments $ACC_{1\text{-}13}$, E_8 under various pH conditions and in the presence and absence of Ca^{2+} (10-fold molar excess) probed by ThT fluorescence assay. (B-C) Infrared spectra of aggregates collected at the end of the kinetic experiment, positions of the amide I band maxima are indicated in parenthesis. (D) Infrared spectra of E_8 and $E_{8(L/D)}$ peptides (0.3 mg/ml, pH 4) subjected to 48h incubation at 60 ºC.

Figure 4. AFM amplitude images of aggregates of $ACC_{1\text{-}13}E_8$ (A) and $ACC_{1\text{-}13}E_{8(L/D)}$ (B) formed at pH 4 and in the absence of Ca^{2+}, and of $ACC_{1\text{-}13}E_{8(L/D)}$ at pH 6.1 and in the presence of 10-fold molar excess of Ca^{2+} (C). Superimposed are cross-sections of selected specimen.

Figure 5. Far-UV CD spectra of (top panel) dissolved $ACC_{1\text{-}13}E_8$ and $ACC_{1\text{-}13}E_{8(L/D)}$ peptides prior to aggregation and before and after acidification, (bottom) $ACC_{1\text{-}13}E_8$ dissolved at pH 6.1 in the presence of increasing molar excess of Ca^{2+} (peptide concentration 0.21 mg/ml, 1 mm quartz cuvette).

Figure 6. Scheme of the aggregation pathways of the peptides investigated in this study. According to the IR data fibrils of $ACC_{1\text{-}13}E_{8(L/D)}$, $ACC_{1\text{-}13}E_8$, and $ACC_{1\text{-}13}$ consist of parallel β-sheet structure. As a separate entity, E_8 peptide forms antiparallel β-sheets with the untypical hydrogen bonds involving bifurcating carbonyl acceptors whereas $E_{8(L/D)}$ is not amyloidogenic at all.